LANGMUIR Article
Cite This: Langmuir 2018, 34, 1340−1346
pubs.acs.org/Langmuir

Modeling Nanoparticle Dispersion in Electrospun Nanofibers

Christopher Balzer,[†] Mitchell Armstrong,[†] Bohan Shan,[†] Yingjie Huang,[‡] Jichang Liu,*[,‡] and Bin Mu*[,†]

[†]Chemical Engineering, School for Engineering of Matter, Transport, and Energy, Arizona State University, 501 East Tyler Mall, Tempe, Arizona 85287, United States

[‡]State Key Laboratory of Chemical Engineering, East China University of Science and Technology, Shanghai 200237, China

Supporting Information

ABSTRACT: The quality of nanoparticle dispersion in a polymer matrix significantly influences the macroscopic properties of the composite material. Like general polymer−nanoparticle composites, electrospun nanofiber nanoparticle composites do not have an adopted quantitative model for dispersion throughout the polymer matrix, often relying on a qualitative assessment. Being such an influential property, quantifying dispersion is essential for the process of optimization and understanding the factors influencing dispersion. Here, a simulation model was developed to quantify the effects of nanoparticle volume loading (ϕ) and fiber-to-particle diameter ratios (D/d) on the dispersion in an electrospun nanofiber based on the interparticle distance. A dispersion factor is defined to quantify the dispersion along the polymer fiber. In the dilute regime (ϕ < 20%), three distinct regions of the dispersion factor were defined with the highest quality dispersion shown to occur when geometric constraints limit fiber volume accessibility. This model serves as a standard for comparison for future experimental studies and dispersion models through its comparability with microscopy techniques and as a way to quantify and predict dispersion in electrospinning polymer−nanoparticle systems with a single performance metric.

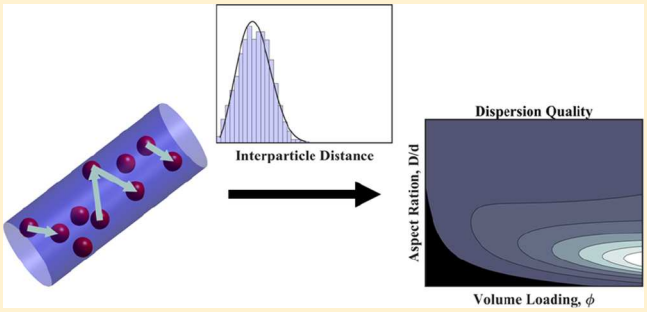

INTRODUCTION

Polymers have been increasingly studied for their applications in nanotechnology and many other fields because of their ease of processing, low cost, and tunability of mechanical and chemical properties.[1] The extensive use and benefits of polymers have led to a need to control and augment their physical and chemical properties. Polymer nanocomposites (PNCs) created through the inclusion of nanoparticles (NPs) into a polymer matrix offer enhanced properties over a pure polymer.[2] Accordingly, PNC applications range from polymer biomaterials,[3] drug delivery,[4] purification processes,[5] and chemical protection.[2] However, the inability to control the dispersion of NPs throughout a polymer matrix is a major setback in adopting the widespread use of PNCs.

The dispersion state (evenly dispersed, randomly dispersed, or clustered) plays a major role in determining the macroscopic effect of NPs in a polymer.[6] Random dispersion is defined as a state in which the particles have no spatial preference but cannot overlap other particles. Evenly dispersed NPs are highly ordered, maximizing the distance between particles and are considered more dispersed than a random system. Clustered states are considered more agglomerated than the random system (Figure 1). NPs aggregate because of their strong interparticle interactions compared to those of the NP−polymer interactions.[7] This is especially true in solvent-based processes, where the high stresses during solvent evaporation in PNCs cause dewetting of polymers from the NP surface.[8] In these instances, aggregation not only prevents the intended property enhancement but also voids the surrounding aggregated NP regions, giving rise to crack formation and material failure.[7] Groups have shown individual cases of improved dispersion. For example, the improved dispersion of silica NPs in solvent casting using methyl ethyl ketone (MEK) over pyridine because of the favorable adsorption of poly(2-vinylpyridine) to silica in MEK.[9] Horrocks et al. showed that the ultrasonic treatment of polypropylene/nanoclay compound melts showed an improved dispersion via high shear forces, but there was no clear improvement for polyamide 6.[10]

To move toward the industrial feasibility of PNCs, a robust systematic method must be adopted for achieving uniform dispersion in PNC systems. Electrospun PNCs have shown promise in limiting/removing the effects of NP aggregation[11] because of the high shear force and electrostatic repulsion present in the electrospinning process.[12] Electrospinning is the process of using electrostatic forces to form fibers (Figure 2). As a result of the simultaneous fiber formation and drying step, NPs cannot agglomerate once the fiber is formed. Because the

Received: October 26, 2017
Revised: December 24, 2017
Published: January 2, 2018

DOI: 10.1021/acs.langmuir.7b03726
Langmuir 2018, 34, 1340−1346

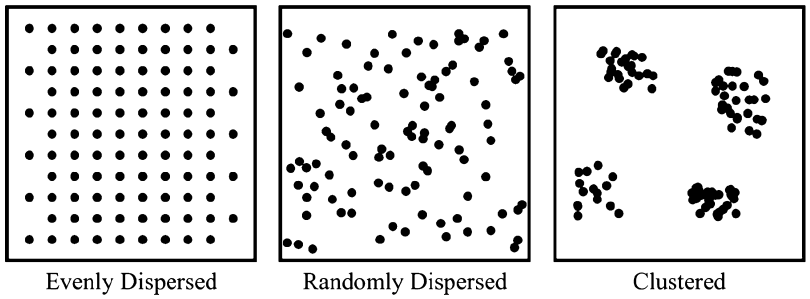

Figure 1. Visual representation of evenly dispersed, randomly dispersed, and clustered dispersion states.

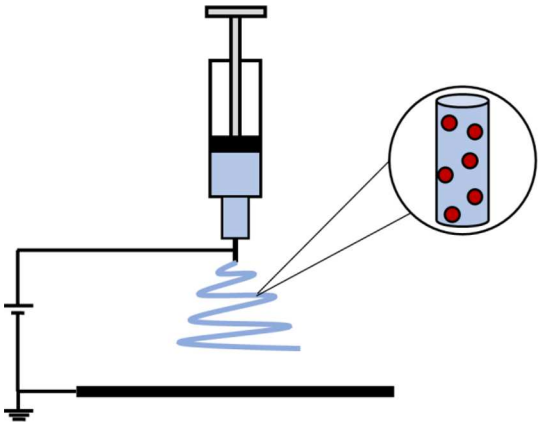

Figure 2. Electrospinning process depiction. The potential difference between the syringe needle and the substrate drives the Taylor cone and fiber formation. The inset depicts a polymer fiber with NPs distributed throughout.

high shear force and repulsion are inherent to the electrospinning process, this dispersion process is compatible for any NP−polymer combination as long as fibers are formed. In fact, many electrospun nanofiber NP composites (ENNCs) have qualitatively been reported to have high degrees of dispersion, as observed in microscopic images, yet a quantitative benchmark or comparison for good dispersion is not defined. Without a model or quantitative benchmark, there is limited ability to fully understand or manipulate dispersion experimentally. The insights gained from a quantitative assessment of dispersion can guide future experiments and can be used in conjunction with the experimental results.

Others have modeled[13] and quantified[14] agglomeration in other polymer−NP systems, but there have been no studies modeling or optimizing the effects of fiber geometry and NP volume loading on the NP dispersion throughout an electrospun fiber. Both volume loading and fiber−particle diameter ratio are variables that encompass many operating parameters of all ENNCs, such as NP preparation methods, concentration, volatility of the solvent, polymer conductivity, solution flow rate, applied voltage, nozzle-collector distance, and even ambient conditions.[15] Here, we model the interparticle distance of randomly distributed spherical NPs along a cylindrical polymer fiber as a function of volume loading (ϕ) and fiber−particle diameter ratio (D/d). Our objective is not only to gain quantitative insights but also to do so in a way that is experimentally accessible. To that end, the scheme to calculate the interparticle distance is transferrable to the two-dimensional (2D) images of ENNCs, and we quantify the quality of dispersion along the fiber with a single metric, the dispersion factor (β). The benefits of this defined dispersion factor are twofold: first, it may help to guide the rational design of ENNCs toward a desired dispersion quality.[16,17] Second, the dispersion factor may serve as a benchmark to compare the degree of dispersion in an ENNC in a systematic and quantitative manner.[18] The model and interparticle distance scheme are the first to exploit the individual fibers in quantifying a long-range dispersion in a mat or film—a method that can be used in future models.

METHODOLOGY

The packing algorithm is sequential in which the NPs (spheres) are placed one at a time in the polymer fiber (cylinder). After inputting D/d, ϕ, and the number of particles generated (n), the volume of the polymer cylinder (V_c) can be calculated, where d is taken to be 1.

$$V_c = \frac{\pi n}{6\phi} d^3$$

The height (h) of the finite cylinder can be calculated from the cylinder volume and the D/d ratio. The method for packing follows a hard sphere model, where particle−particle interactions are neglected and follow the below potential model, where r_i and r_j are the particle locations.

$$V(r_i, r_j) = \begin{cases} 0 & \text{if } |r_i - r_j| \geq d \\ \infty & \text{if } |r_i - r_j| < d \end{cases}$$

The particles are bound inside of the Cartesian cylinder, limiting the particle center locations to $x_i^2 + y_i^2 \leq D - d/2$ and $d/2 \leq z \leq h - d/2$ (Figure 3). Possible particle locations are generated for each particle and then checked against the potential function to ensure no particles overlap the previously generated particles. A random nonoverlapping location is selected, and the cycle repeats to place the next particle. See the Supporting Information for the annotated simulation code.

After generating the particles, the interparticle distance, ωd, is calculated along the fiber. Several others[19−21] have used the interparticle distance as a measure of NP dispersion. When analyzing the large areas of transmission electron microscopy (TEM) images, the mean interparticle distance method is insensitive to the dispersion quality (clustered vs dispersed) and sensitive to the number of NPs.[14] Here, the strong influence of the number of particles is eliminated by only looking at the adjacent particles along a fiber. We define the interparticle distance to be the distance from one particle center to its closest neighbor in a positive axial direction ($+z$). Note that because $d = 1$, the interparticle distance will be represented as ω. Instead of a three-dimensional distance, a 2D projection of the fiber was considered. This is motivated by (1) the

DOI: 10.1021/acs.langmuir.7b03726
Langmuir 2018, 34, 1340−1346

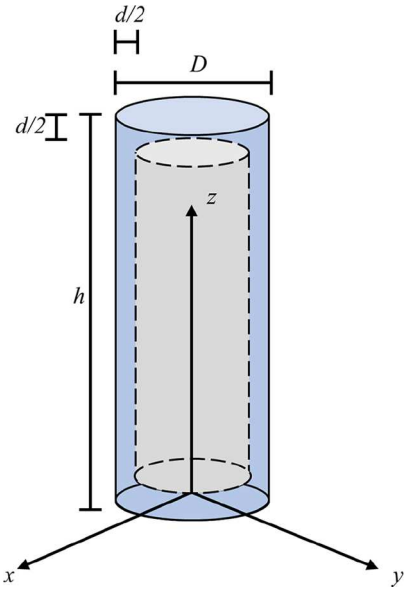

Figure 3. Depiction of the polymer fiber (outer blue cylinder) and possible particle center locations (inner gray cylinder) used in the simulation to place the particles. Note that the fiber lies along the *z*-axis. When calculating the interparticle distance, the *y*-coordinate is neglected.

common experimental equivalent method of using microscopy and image processing software to measure the interparticle distance along the fiber as a 2D image and (2) the fact that the dispersion at a single axial position is secondary to the long-range dispersion along the fiber axis, especially in applications where the permeation direction is perpendicular to the plane of the fiber mat (e.g., purification processes). Figure 4 shows how the fibers are reduced to two dimensions and the scheme to calculate the interparticle distance. Practically, this is done by

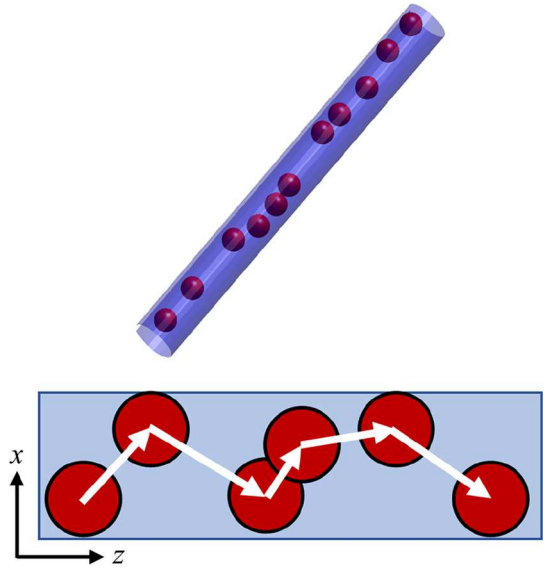

Figure 4. Section of the generated fiber with dispersed particles (top) and 2D projection of the fiber and particles in the *xz*-plane (bottom). Arrows represent the measured interparticle distance. Note that the particles can overlap in the projection, leading to $0 \leq \omega \leq 1$ for the overlapping particles.

only considering the distance in the *xz*-plane. Values of ω can range from 0 to infinity as particles can overlap in the *xz*-plane.

Key Assumptions and Limitations. By nature of the packing scheme, the particles are not guided into energetically favorable or ideal packing configurations or moved once placed. This reflects how the viscous nature of the polymer prevents settling of NPs once the fiber is formed. Consequently, for each D/d, there is a maximum ϕ that is lower than the other numerically computed sphere in the cylinder packing configurations[22−24] and lower than the random close or loosely packed systems.[25]

The particles are assumed not to interact via repulsion or attraction. As discussed above, NPs tend to aggregate to limit the particle−polymer surface energy. However, in the electrospinning process, the induced interparticle repulsion opposes this attraction. The effect of attraction/repulsion is considered to be net zero. Additionally, as particles leave the needle, the geometric confinement coupled with high shear and repulsive forces can force the particles to partially exit the fiber, causing surface exposure. This process happens at loadings where the particles are kinetically trapped and cannot find a favorable position in the fiber before solidifying.[26] Accordingly, the most appropriate use of the models developed is the dilute case of low loading (<20% by volume) and D/d, where the particles are considered isolated.

Interparticle Distance Analysis and Dispersion Factor, β. Simulation runs were conducted over a range of aspect ratios and loading values. Distributions of the interparticle distance were developed from the results of 10 runs of 500 particles (5000 total) for a given D/d and ϕ combination. The distributions were fit to the Weibull distribution, where the probability density function is represented as

$$f(\omega;\lambda,k) = \begin{cases} \frac{k}{\lambda}\left(\frac{\omega}{\lambda}\right)^{k-1} e^{-(\omega/\lambda)^k} & \omega \geq 0 \\ 0 & \omega < 0 \end{cases}$$

where λ is the shape parameter and k is the scale parameter. The Weibull distribution aligns with a kernel density estimate and has physically realizable values for the interparticle distance (see the Supporting Information for detailed discussion). From the probability density function, the mean and variance are given as follows.

$$\mu = \lambda\Gamma\left(1 + \frac{1}{k}\right)$$

$$\sigma^2 = \lambda^2\left[\Gamma\left(1 + \frac{2}{k}\right) - \left(\Gamma\left(1 + \frac{1}{k}\right)\right)^2\right]$$

A dispersion factor (β) is defined to quantify the dispersion for different combinations of aspect ratios and loading. The dispersion factor is the ratio of mean to SD of the interparticle distance and the inverse of the coefficient of variation.

$$\beta = \frac{\mu}{\sigma}$$

The dispersion factor can be used to guide the electrospinning operating parameters for a certain volume loading or diameter ratio, where the larger values represent better dispersion along the fiber. The quantity favors high control (low σ) but discriminates against clustering, where σ may be small and μ is also small. For the systems where the dispersion

DOI: 10.1021/acs.langmuir.7b03726
Langmuir 2018, 34, 1340−1346

is predominately in a single axial position along the fiber (large D/d), the smaller values of μ tend to decrease the dispersion factor. In that way, the dispersion factor is an easy-to-interpret single value with a physical significance that can be used to guide electrospinning operating parameters for a certain volume loading or diameter ratio.

RESULTS AND DISCUSSION

Influence of the Fiber-to-Particle Diameter Ratio, *D/d*.

With a uniform probability distribution, the aspect ratio (D/d) greatly influences the available sites for placing the particle centers. From a geometric standpoint, there are two regions of the aspect ratio. These regions can be characterized by their respective maximum ϕ values. The first range occurs with aspect ratios of $1 \leq D/d \leq 1.4$ and $D/d \geq 2.2$, where volume loading values over 25% are possible [$\phi_{max}(1) = 50\%$, $\phi_{max}(1.4)$, and $\phi_{max}(2.2) = 25\%$]. From $1 \leq D/d \leq 1.4$, two particles cannot be distributed at the same axial position in the fiber. The excluded volume from each particle placement is relatively small. Above $D/d = 2.2$, the particle centers gain access to the additional dimension of the fiber. The second range of $1.4 < D/d \leq 2.2$ occurs, where the geometric confinement leads to low maximum loadings ($\phi_{max} \leq 25\%$). The confinement is illustrated in 2D in Figure 5, where the placement of a particle in the $D/d = 2$ fiber removes twice the available volume/area as in $D/d = 1$. As the aspect ratio increases further, the wall effects and confinement drastically reduce (Figure 5). These results from the random distribution of the particles mirror the simulation studies[23] of ideal sphere packing in cylinders, where ϕ_{max} drops significantly from $1.4 < D/d \leq 2.2$. Further explanation and visuals of the wall effects are given in the Supporting Information.

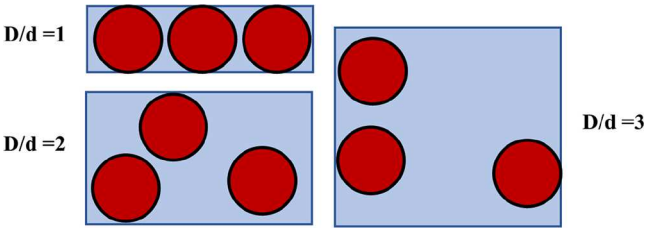

Figure 5. 2D depiction of geometric confinement/wall effects. When $D/d = 1$ and 3, placement of a particle only restricts new particles from being placed within a distance d. No dead zones are created. Placing a particle for the case for $D/d = 2$ significantly limits the accessible area because of the fiber wall.

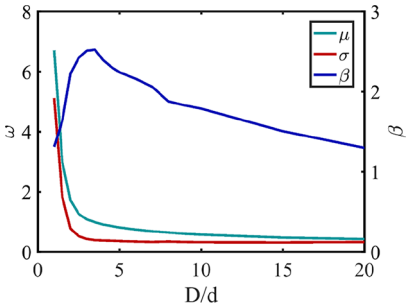

Figure 7. Mean and SD of ω and β as a function of the aspect ratio for a volume loading of 10%.

The effect of the aspect ratio on the interparticle distance distribution was determined by varying the aspect ratio at a constant volume loading. Figure 6 shows the resulting distributions for the aspect ratios from 1 to 4 at a constant volume loading of 10%. At the lowest aspect ratio, the particles were dispersed at high variable distances. Less than 5% of the particles were touching at this value of ϕ. As the aspect ratio increases, particles are forced to be closer as the fiber length decreases. For $D/d = 2$, 20% of the particles have $\omega \approx 1$, indicating that the particles are adjacent and lined along the fiber axis. Additionally, very few particles have $\omega < 1$, which is consistent with the previous discussion of wall effects. As wall effects become less prevalent, more particles can occupy the

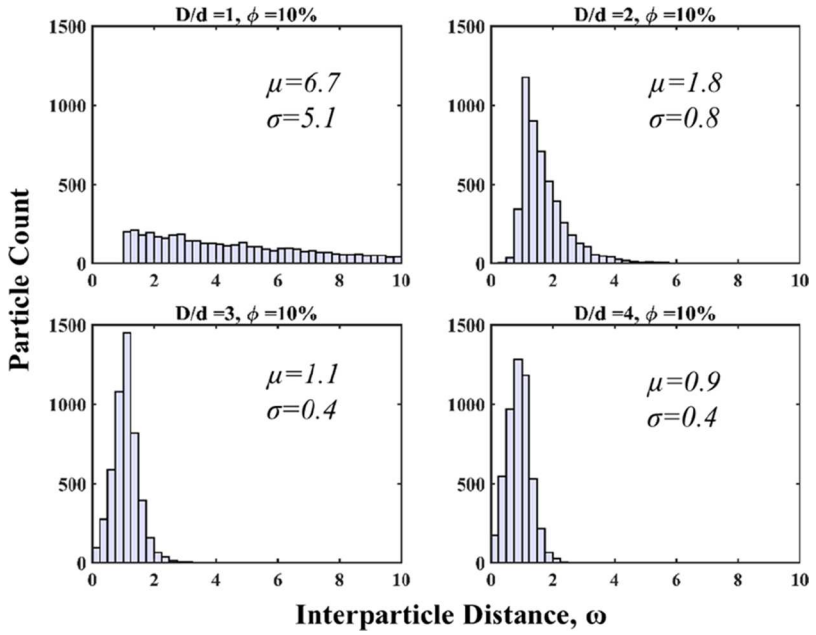

Figure 6. Interparticle distance distributions (top row) with $D/d = 1$, 2, 3, and 4 (left to right) at constant $\phi = 10\%$. The distributions result from 10 runs of 500 particles. Mean and SD calculated from the Weibull distribution. The bottom row depicts a fiber segment for each case.

DOI: 10.1021/acs.langmuir.7b03726
Langmuir 2018, 34, 1340−1346

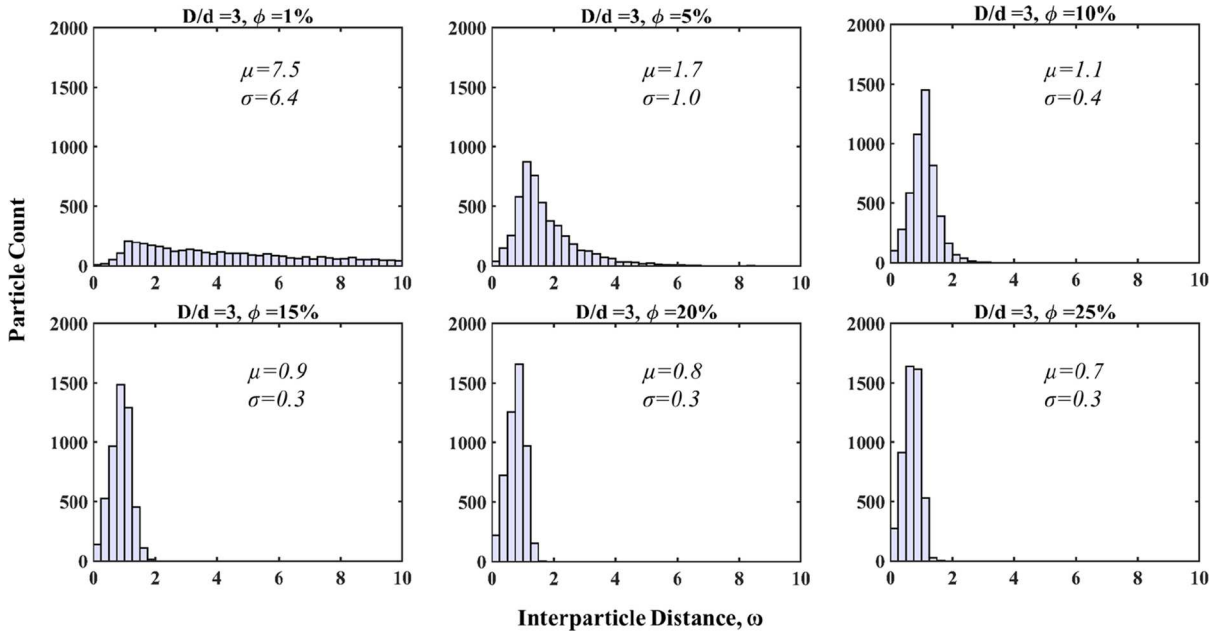

Figure 8. Interparticle distance distributions with D/d = 3 at constant ϕ = 1, 5, and 10% (top) and 15, 20, and 25% (bottom). Distributions from 10 runs of 500 particles. The mean and SD were calculated from the Weibull distribution.

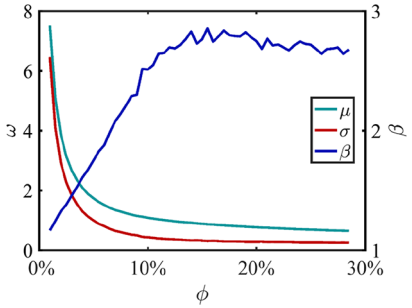

Figure 9. Mean and SD of ω as a function of ϕ for D/d = 3 and dispersion factor β as a function of ϕ.

same axial position, driving μ and σ down and below 1. See Figures S3–S7 for the generated fiber and fiber projection visuals.

The overall relationship for ϕ = 10% is shown in Figure 7. As $D/d \rightarrow \infty$, the mean and SD of the interparticle distance approach zero, as all particles are forced into the same plane. Figure 7 also shows the dispersion factor (β) for a volume loading of 10%. When σ is large, as with D/d = 1, the particles may be far apart, but the varying interparticle distance still creates unbalanced regions of particles that could lead to voids, not solving the dispersion issue. The ideal scenario occurs when the SD is small and the mean distance is large—particles spread out from each other to a controllable, consistent distance. The maximum β for ϕ = 10% occurs at approximately D/d = 3, where particles will still have some wall effects, but the confinement promotes dispersion along the axis. Intuitively, different volume loadings will have different maximum values of β, as unique loadings are subject to unique wall effects at each aspect ratio. The maximum β will arise where those wall effects dominate, which is discussed in more detail below.

Influence of Volume Loading, ϕ. The maximum volume loading of spheres in cylinders has been studied for many industrial applications, particularly those involving granular matter.[27] With viscous fluid surrounding the NPs, they are

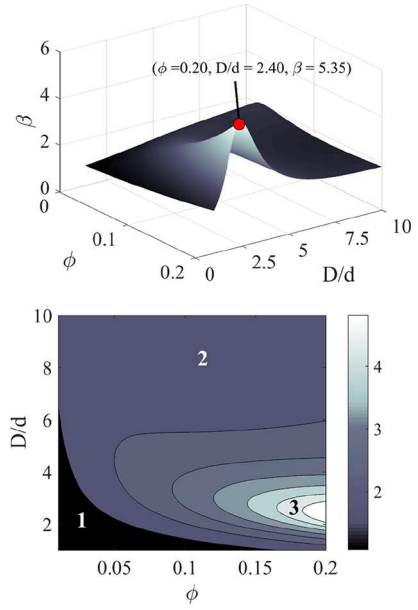

Figure 10. Surface (top) and contour (bottom) of the dispersion factor β over the range of D/d from 0 to 10 and ϕ from 1 to 20%. Three regions of (1) low-, (2) medium-, and (3) high-dispersion quality are labeled on the contour map.

kinetically and energetically limited from repositioning to the ideal packing at high loadings. The effect of volume loading on the interparticle distance at constant D/d is shown in Figure 8. As the loading increases, the particles are forced to occupy a smaller space. At ϕ = 0.01, less than 5% of the particles are touching. The number of touching particles significantly increases, even for ϕ = 0.05, with nearly 20% of the particles touching ($\omega \approx 1$) along the length of the fiber. For large enough aspect ratios, the particles will increasingly overlap in the xz-plane. For each D/d, the distribution shape and scaling factors remain essentially constant past a threshold loading value.

DOI: 10.1021/acs.langmuir.7b03726
Langmuir 2018, 34, 1340−1346

For PNCs, the percolation threshold determines when the NPs begin influencing macroscopic properties. The percolation threshold is governed by the macroscopic property of interest (i.e., mechanical or electrical) and the polymer−NP system.[28] Percolation thresholds have been extensively studied for the conducting polymer composites using computational and analytical methods.[29] As seen in Figure 8, the mean dispersion along the fiber does not significantly change at higher loadings. In terms of operability, there is a range of acceptable volume loading values to tune the desired macroscopic properties until the percolation limit, where the NPs can degrade the mechanical properties of the polymer. In this range, there is not a large trade-off between optimum dispersion and ϕ. The dispersion factor values in Figure 9 reflect this range. Volume loadings greater than 14% show a dispersion factor leveling off to a less dynamic behavior, an approximately constant value as the loading approaches ϕ_{max} for $D/d = 3$. The variability in β is a result of the variations in μ and σ and sensitivity to σ in calculating β, given the sample set of 10 runs of 500 particles.

Empirical Model for Coefficients μ and σ. To predict the dispersion over the dilute range of ϕ and D/d, an empirical model was fit to the mean and SD of the interparticle distance. The models below apply to $1 \leq D/d \leq 10$ and $0.01 \leq \phi \leq 0.20$. The coefficients were determined using least squares. Bisquare weighting was used to reduce the influence of extreme values on the model fit.

$$\mu = 0.3736 + \left(-2.486\, e^{-0.9654(D/d)} + 0.8548\, e^{-25.12\phi} + \frac{0.5429}{(D/d)^{2.136}\phi^{1.047}}\right) e^{2.093\phi(D/d)^{0.5}}$$

$$\sigma = 0.2087 + \left(-2.264\, e^{-0.444(D/d)} + 0.1991 + \frac{0.6261}{(D/d)^{2.132}\phi^{1.009}}\right) e^{-1.607\phi^{1.5}(D/d)}$$

As seen in Figure 10, there are three distinct regions of the dispersion factor: (1) low loading and low aspect ratio that result in particles being far apart at varying distances; (2) high diameter ratio, where the particles tend not to disperse along the fiber as much as in the diameter of the fiber, or medium loadings where the particles are not at a controllable distance from each other; and (3) maximum β values, where confinement forces the particles to disperse along the fiber without a significant variation. The maximum dispersion factor of 5.35 occurs at $D/d = 2.4$ with a loading of 20%. From these regions, the main determination of dispersion quality is the presence of wall effects or dead zones, which promote dispersion along the fiber.

Both equations can be compared to the experimentally observed dispersion along a polymer fiber as a quantitative systematic measure of dispersion in an actual fiber material. With the most common characterization technique of fiber composites being microscopy, such as TEM, confocal microscopy, and scanning electron microscopy with energy-dispersive X-ray spectrometry, one can measure the interparticle distance using image processing software, such as ImageJ.[30] By computing the dispersion factor, one can compare to the hard sphere value to gauge the factors that would cause the particles to nonrandomly distribute, namely, favorable particle−particle interactions. The empirical equations are also useful in guiding the design parameters of an ENNC system to target optimal dispersion.

Particle−Particle Interactions. Although not studied here, the presence of particle−particle interactions would influence the interparticle distance. One can imagine clusters forming in the fiber, much like the film depicted in Figure 1. With increasing interactions, the interparticle distance is expected to decrease from the hard sphere case, as the particles prefer to be closer to one another; however, clusters will leave the significant voids along the length of the fiber. When analyzing the distribution of ω, one would expect a multimodal distribution arising from clusters and voids. For such a system, μ would be lower than a noninteracting system because of close clusters, but σ would be higher, driving down the dispersion factor. These are important characteristics to keep in mind when looking at the dispersion factor of an experimental system, possibly to compare the relative strengths of interaction.

CONCLUSIONS

With electrospinning being a viable solution for creating well-dispersed polymer−NP matrices, a model of the dispersion is essential for experimental comparisons and understanding the role of processing parameters on dispersion. A simulation was developed to analyze the interparticle distance of NPs distributed in an electrospun nanofiber. The distributions of the interparticle distance were analyzed to find whether the ideal dispersion has characteristics of high mean values but a low variance in the interparticle distances. The best dispersion, corresponding to the highest dispersion factor value (β), occurs where geometric confinement creates dead zones and forces particles to more uniformly align on the axis of the fiber. The counting scheme for the interparticle distance described here is highly compatible with current microscopy methods already used to characterize nanocomposite fibers and current image-processing capabilities. The empirical two-parameter model can be used to predict experimental dispersion in a quantifiable way and can serve as a standard for comparison to probe the effects of both interparticle attraction and polymer−particle interaction.

ASSOCIATED CONTENT

Supporting Information

The Supporting Information is available free of charge on the ACS Publications website at DOI: 10.1021/acs.langmuir.7b03726.

Complete MATLAB simulation code, dead zone/excluded volume discussion, probability distribution discussion, and generated fiber/projection images (PDF)

AUTHOR INFORMATION

Corresponding Authors

*E-mail: liujc@ecust.edu.cn (J.L.).
*E-mail: bmu@asu.edu (B.M.).

ORCID

Jichang Liu: 0000-0002-5295-1778
Bin Mu: 0000-0002-9117-1299

Notes

The authors declare no competing financial interest.

DOI: 10.1021/acs.langmuir.7b03726
Langmuir 2018, 34, 1340−1346

■ ACKNOWLEDGMENTS

This research work was financially supported by Arizona State University and the National Science Foundation (Grant Number 1748641). We also acknowledge the use of computing resources from ASU Research Computing Center.

■ REFERENCES

(1) Li, H.; Huck, W. T. S. Polymers in Nanotechnology. *Curr. Opin. Solid State Mater. Sci.* **2002**, *6*, 3−8.
(2) Paul, D. R.; Robeson, L. M. Polymer Nanotechnology: Nanocomposites. *Polymer* **2008**, *49*, 3187−3204.
(3) Hule, R. A.; Pochan, D. J. Polymer Nanocomposites for Biomedical Applications. *MRS Bull.* **2007**, *32*, 354−358.
(4) DeLeon, V. H.; Nguyen, T. D.; Nar, M.; D'Souza, N. A.; Golden, T. D. Polymer Nanocomposites for Improved Drug Delivery Efficiency. *Mater. Chem. Phys.* **2012**, *132*, 409−415.
(5) Cong, H.; Radosz, M.; Towler, B.; Shen, Y. Polymer−Inorganic Nanocomposite Membranes for Gas Separation. *Sep. Purif. Technol.* **2007**, *55*, 281−291.
(6) Jancar, J.; Douglas, J. F.; Starr, F. W.; Kumar, S. K.; Cassagnau, P.; Lesser, A. J.; Sternstein, S. S.; Buehler, M. J. Current Issues in Research on Structure−Property Relationships in Polymer Nanocomposites. *Polymer* **2010**, *51*, 3321−3343.
(7) Šupová, M.; Martynková, G. S.; Barabaszová, K. Effect of Nanofillers Dispersion in Polymer Matrices: A Review. *Sci. Adv. Mater.* **2011**, *3*, 1−25.
(8) Duval, J. Adsorbent Filled Polymeric Membranes. Ph.D. Thesis, University of Twente, The Netherlands, 1995.
(9) Jouault, N.; Zhao, D.; Kumar, S. K. Role of Casting Solvent on Nanoparticle Dispersion in Polymer Nanocomposites. *Macromolecules* **2014**, *47*, 5246−5255.
(10) Horrocks, A. R.; Kandola, B.; Milnes, G. J.; Sitpalan, A.; Hadimani, R. L. The Potential for Ultrasound to Improve Nanoparticle Dispersion and Increase Flame Resistance in Fibre-Forming Polymers. *Polym. Degrad. Stab.* **2012**, *97*, 2511−2523.
(11) Zhang, C.-L.; Yu, S.-H. Nanoparticles Meet Electrospinning: Recent Advances and Future Prospects. *Chem. Soc. Rev.* **2014**, *43*, 4423−4448.
(12) Bian, S.; Jayaram, S.; Cherney, E. A. Electrospinning as a New Method of Preparing Nanofilled Silicone Rubber Composites. *IEEE Trans. Dielectr. Electr. Insul.* **2012**, *19*, 777−785.
(13) Liu, J.; Gao, Y.; Cao, D.; Zhang, L.; Guo, Z. Nanoparticle Dispersion and Aggregation in Polymer Nanocomposites: Insights from Molecular Dynamics Simulation. *Langmuir* **2011**, *27*, 7926−7933.
(14) Khare, H. S.; Burris, D. L. A Quantitative Method for Measuring Nanocomposite Dispersion. *Polymer* **2010**, *51*, 719−729.
(15) Pisignano, D. *Polymer Nanofibers: Building Blocks for Nanotechnology*, 1st ed.; Royal Society of Chemistry, 2013.
(16) Armstrong, M. R.; Shan, B.; Maringanti, S. V.; Zheng, W.; Mu, B. Hierarchical Pore Structures and High ZIF-8 Loading on Matrimid Electrospun Fibers by Additive Removal from a Blended Polymer Precursor. *Ind. Eng. Chem. Res.* **2016**, *55*, 9944−9951.
(17) Armstrong, M. R.; Arredondo, K. Y. Y.; Liu, C.-Y.; Stevens, J. E.; Mayhob, A.; Shan, B.; Senthilnathan, S.; Balzer, C. J.; Mu, B. UiO-66 MOF and Poly(vinyl Cinnamate) Nanofiber Composite Membranes Synthesized by a Facile Three-Stage Process. *Ind. Eng. Chem. Res.* **2015**, *54*, 12386−12392.
(18) Armstrong, M. R.; Shan, B.; Mu, B. Microscopy Study of Morphology of Electrospun Fiber-MOF Composites with Secondary Growth. *MRS Adv.* **2017**, *2*, 2457−2463.
(19) Basu, S. K.; Tewari, A.; Fasulo, P. D.; Rodgers, W. R. Transmission Electron Microscopy Based Direct Mathematical Quantifiers for Dispersion in Nanocomposites. *Appl. Phys. Lett.* **2007**, *91*, 053105.
(20) Tyson, B. M.; Abu Al-Rub, R. K.; Yazdanbakhsh, A.; Grasley, Z. A Quantitative Method for Analyzing the Dispersion and Agglomeration of Nano-Particles in Composite Materials. *Composites, Part B* **2011**, *42*, 1395−1403.
(21) Hamming, L. M.; Qiao, R.; Messersmith, P. B.; Brinson, L. C. Effects of Dispersion and Interfacial Modification on the Macroscale Properties of TiO2 Polymer-Matrix Nanocomposites. *Compos. Sci. Technol.* **2009**, *69*, 1880−1886.
(22) Fu, L.; Steinhardt, W.; Zhao, H.; Socolar, J. E. S.; Charbonneau, P. Hard Sphere Packings within Cylinders. *Soft Matter* **2016**, *12*, 2505−2514.
(23) Mughal, A.; Chan, H. K.; Weaire, D.; Hutzler, S. Dense Packings of Spheres in Cylinders: Simulations. *Phys. Rev. E: Stat., Nonlinear, Soft Matter Phys.* **2012**, *85*, 051305.
(24) Mueller, G. E. Numerically Packing Spheres in Cylinders. *Powder Technol.* **2005**, *159*, 105−110.
(25) Baranau, V.; Tallarek, U. Random-Close Packing Limits for Monodisperse and Polydisperse Hard Spheres. *Soft Matter* **2014**, *10*, 3826−3841.
(26) Armstrong, M.; Balzer, C.; Shan, B.; Mu, B. Influence of Particle Size and Loading on Particle Accessibility in Electrospun Poly(ethylene Oxide) and ZIF-8 Composite Fibers: Experiments and Theory. *Langmuir* **2017**, *33*, 9066−9072.
(27) Radin, C. Random Close Packing of Granular Matter. *J. Stat. Phys.* **2008**, *131*, 567−573.
(28) Penu, C.; Hu, G.-H.; Fernandez, A.; Marchal, P.; Choplin, L. Rheological and Electrical Percolation Thresholds of Carbon Nanotube/polymer Nanocomposites. *Polym. Eng. Sci.* **2012**, *52*, 2173−2181.
(29) Li, J.; Kim, J.-K. Percolation Threshold of Conducting Polymer Composites Containing 3D Randomly Distributed Graphite Nanoplatelets. *Compos. Sci. Technol.* **2007**, *67*, 2114−2120.
(30) Rueden, C. T.; Schindelin, J.; Hiner, M. C.; DeZonia, B. E.; Walter, A. E.; Arena, E. T.; Eliceiri, K. W. ImageJ2: ImageJ for the next generation of scientific image data. *BMC Bioinf.* **2017**, *18*, 529.

DOI: 10.1021/acs.langmuir.7b03726
Langmuir 2018, 34, 1340−1346